



Derivation of salt content in salinized soil from hyperspectral reflectance data: A case study at Minqin Oasis, Northwest China

QIAN Tana^{1*}, Atsushi TSUNEKAWA¹, PENG Fei¹, Tsugiyuki MASUNAGA², WANG Tao³, LI Rui⁴

¹ Arid Land Research Center, Tottori University, Tottori 680-0001, Japan;

² Life and Environmental Science, Shimane University, Matsue 690-8504, Japan;

³ Key Laboratory of Desert and Desertification, Northwest Institute of Eco-Environment and Resources, Chinese Academy of Sciences, Lanzhou 730000, China;

⁴ State Key Laboratory of Remote Sensing Science, Institute of Remote Sensing and Digital Earth, Chinese Academy of Sciences, Beijing 100101, China

Abstract: Soil salinization is a serious ecological and environmental problem because it adversely affects sustainable development worldwide, especially in arid and semi-arid regions. It is crucial and urgent that advanced technologies are used to efficiently and accurately assess the status of salinization processes. Case studies to determine the relations between particular types of salinization and their spectral reflectances are essential because of the distinctive characteristics of the reflectance spectra of particular salts. During April 2015 we collected surface soil samples (0–10 cm depth) at 64 field sites in the downstream area of Minqin Oasis in Northwest China, an area that is undergoing serious salinization. We developed a linear model for determination of salt content in soil from hyperspectral data as follows. First, we undertook chemical analysis of the soil samples to determine their soluble salt contents. We then measured the reflectance spectra of the soil samples, which we post-processed using a continuum-removed reflectance algorithm to enhance the absorption features and better discriminate subtle differences in spectral features. We applied a normalized difference salinity index to the continuum-removed hyperspectral data to obtain all possible waveband pairs. Correlation of the indices obtained for all of the waveband pairs with the wavebands corresponding to measured soil salinities showed that two wavebands centred at wavelengths of 1358 and 2382 nm had the highest sensitivity to salinity. We then applied the linear regression modelling to the data from half of the soil samples to develop a soil salinity index for the relationships between wavebands and laboratory measured soluble salt content. We used the hyperspectral data from the remaining samples to validate the model. The salt content in soil from Minqin Oasis were well produced by the model. Our results indicate that wavelengths at 1358 and 2382 nm are the optimal wavebands for monitoring the concentrations of chlorine and sulphate compounds, the predominant salts at Minqin Oasis. Our modelling provides a reference for future case studies on the use of hyperspectral data for predictive quantitative estimation of salt content in soils in arid regions. Further research is warranted on the application of this method to remotely sensed hyperspectral data to investigate its potential use for large-scale mapping of the extent and severity of soil salinity.

Keywords: salinity index; soil salt content; spectral reflectance; waveband pairs; arid regions

Citation: QIAN Tana, Atsushi TSUNEKAWA, PENG Fei, Tsugiyuki MASUNAGA, WANG Tao, LI Rui. 2019. Derivation

*Corresponding author: QIAN Tana (E-mail: qian.tana@gmail.com)

Received 2017-12-29; revised 2018-04-03; accepted 2018-05-17

© Xinjiang Institute of Ecology and Geography, Chinese Academy of Sciences, Science Press and Springer-Verlag GmbH Germany, part of Springer Nature 2019

of salt content in salinized soil from hyperspectral reflectance data: A case study at Minqin Oasis, Northwest China. *Journal of Arid Land*, 11(1): 111–122. <https://doi.org/10.1007/s40333-019-0091-9>

1 Introduction

Soil salinization is the most common type of land degradation encountered in natural resource management in many parts of the world and has received much attention from farmers, politicians and researchers (Wild, 2003; Farifteh et al., 2006; Rengasamy, 2006; Sheng et al., 2010; Wang et al., 2018). As one of the primary inhibitors of crop yield and ecological functions, soil salinity might ultimately lead to environmental disaster and food crises in arid regions (Munns, 2002; Barrett-Lennard, 2003). In China, the area of salt-affected land (3.6×10^7 hm²) accounts for 4.88% of the country's total available land resource (Li et al., 2014; Zhang, 2014). Given the broad distribution of land salinization in China, it poses a severe threat to the sustainability of regional agriculture (Li et al., 2014).

Soil salinization in China occurs mainly in arid and semi-arid areas in the northwest regions, where low precipitation is coupled with intensive evapotranspiration. The strong evapotranspiration and the ineffective irrigation drainage systems have resulted in the secondary salinization (Ma et al., 2005; Wang et al., 2008). Minqin Oasis, one of the most fragile oasis in Northwest China, suffers a great shortage of fresh water for agriculture because of the low precipitation and massive demand for water created by increased agricultural activity and rapid population growth. Groundwater has been over-exploited to fill the gap between surface freshwater supply and demand (Bondes and Li, 2013; Wei et al., 2016). Groundwater extraction provides short-term relief from the scarcity of water for agricultural and domestic use, but excessive extraction lowers the water table and increases salt content in groundwater (Chen et al., 2016). Long-term agricultural use of saline water has led to a rapid increase of secondary salinization at Minqin Oasis (Chen et al., 2016; Qian et al., 2017). For example, the total area of saline land within Minqin Oasis increased by 541.35 km² from 1991 to 2009 (Xiao et al., 2007; Zhang et al., 2014). The persistent water scarcity and adverse effects of secondary salinization on crop yields led to a cropland abandonment of about 780 hm² (equal to 81% of area under cultivation) at two villages at Minqin Oasis in 2003 (Ma et al., 2007).

The combined effects of spatiotemporal variations of natural conditions (e.g., availability of irrigation water) and the seasonal and annual changes of agricultural practices have made it difficult to reduce the rate of salinization at the regional level in China. Accurate estimates of the areal extent of salinized land and prediction of areas likely to become saline are essential for policy makers, planners and farmers to allow effective management of irrigated land, control of salinization and reversal of current trends of soil and water degradation. Thus, it is crucially important to monitor soil salinity and assess its severity to prevent further degradation of agricultural land (Weng et al., 2010). Because the conventional methods of monitoring salinity by using ground-based geophysical techniques are time-consuming and costly (Dehaan and Taylor, 2003), a number of researchers have attempted to develop more cost-effective approaches to monitor current status of soil salinization and to predict future salinization by using multispectral or hyperspectral reflectance remote sensing techniques. The basis for monitoring the soil salinization is the distinct reflectance of different minerals (Mougenot et al., 1993; Metternicht and Zinck, 2003). Single or multiple wavebands have been selected and mathematically combined (e.g., division and subtraction) into indices to develop models that can be used to monitor large spatial scale of soil salinization (Douaoui et al., 2006; Fernandez-Bucs et al., 2006; Farifteh et al., 2007; Ding et al., 2011).

Comparing with multispectral data, hyperspectral reflectance data can capture subtle differences in soil properties and provide quick indirect assessments of soil characteristics due to the high spectral resolution (10–20 nm) and hundreds of available bands (Ben-Dor and Banin, 1995; Dwivedi, 2001; Farifteh et al., 2006; Gomez et al., 2008; Haubrock et al., 2008a; Zornoza et al., 2008; Ben-Dor et al., 2009; Goetz, 2009). Additionally, due to the ability of providing quantitative information about the particular salt minerals in soils, the development of methods that use

hyperspectral data to estimate soil salinity has been the objective of many studies during the past two decades (Farifteh et al., 2006; Gomez et al., 2008; Haubrock et al., 2008b; Lu et al., 2013). Howari et al. (2002) assessed the spectral reflectance of soils treated with saline solutions containing NaCl, NaHCO₃, NaSO₄, and CaSO₄·H₂O in the laboratory to identify the presence of primary diagnostic spectral features of salt crusts. In addition, the sensitive bands for soil salt estimation vary with the predominant chemical compounds (salt mineralogy) in saline soils (Metternicht and Zinck, 2003; Farifteh et al., 2008; Wang et al., 2012; Fan et al., 2015).

The aim of this study was to estimate the salt content of soils from laboratory-derived hyperspectral data with a linear model. For this purpose, firstly, soil salinity and spectra data were statistically analysed to find optimal wavebands for deriving salt contents in soils. Secondly, a normalized difference spectral index that integrates the optimal wavebands was used to develop a predictive model for estimating the soil salt content from hyperspectral data.

2 Methods

2.1 Study area

The Minqin Oasis (38°09′–39°05′N, 102°24′–103°49′E) is near the border of Gansu Province and Inner Mongolia Autonomous Region in Northwest China. It is bounded to the west by the Badain Jaran Desert and to the east by the Tengger Desert. This part of China has a temperate continental arid climate with a mean annual precipitation of 110 mm and annual evaporation of 2623 mm. The annual mean temperature is 7.8°C with the monthly means ranging from −8.6°C in January to 21.8°C in August. The annual mean wind velocity is 2.7 m/s, and wind force stronger than Beaufort scale 8 (17.2–20.7 m/s) occurs 28 d per year on average. According to the genetic soil classification of China (Shi et al., 2006), the natural soils include grey-brown desert soil, aeolian sandy soil and saline soil. Cultivated soils are mainly irrigated desert soil and fluvo-aquic soils.

The Shiyang River originates from the Qilian Mountains and is the only source of fresh water in Minqin Oasis, which is covered largely by croplands that are heavily reliant on irrigation water from the river. The oasis is divided into five sub-regions: Huqu, Baqu, Shoucheng, Hongsha Liang and Quanshanqu. Our study area is the Huqu sub-region (38°42′–39°05′N, 103°25′–103°49′E) at the northern margin of Minqin Oasis (Fig. 1). The sub-region includes the terminal lake of the Shiyang River. Thus, it is an area with long-term salt accumulation. The location of the sub-region and the inappropriate irrigation practices led to protracted and severe groundwater mineralization, soil salinization and desertification, such that most of the croplands are no longer to sustain grain crops. Substantial cropping areas have been abandoned because of the low productivity caused by the groundwater mineralization (groundwater mineralization >3.0 g/L can cause yield reductions of >10%) (Xiao et al., 2007).

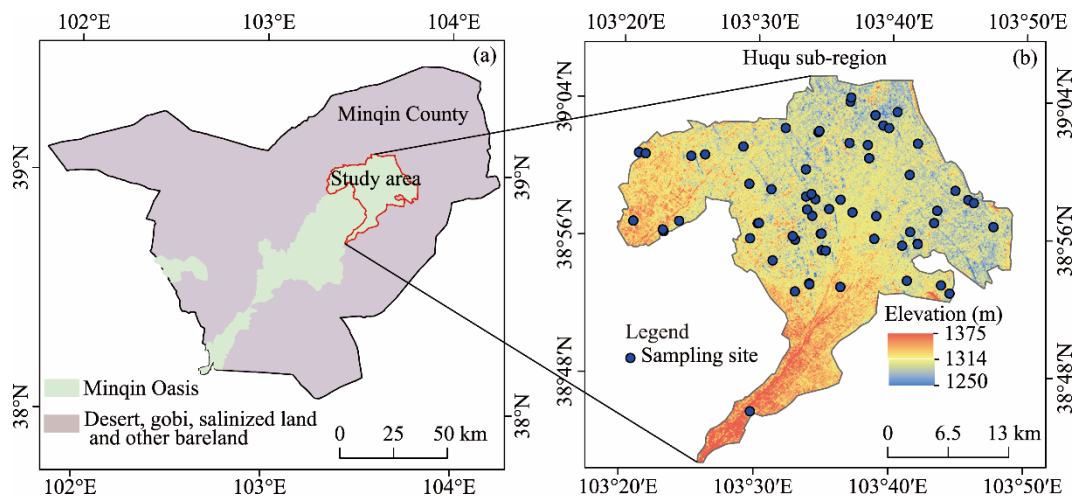


Fig. 1 Location of Minqin Oasis (a) and the sampling sites in the study area, Huqu sub-region (b)

2.2 Sampling and laboratory analysis

The field work was conducted in Huqu sub-region in April 2015 when salt content in the surface soils reach the annual maximum. Soil samples were collected from the upper soil layer (0–10 cm depth) at 64 sites (Fig. 1). At each sampling site, we collected soil samples at five randomly selected locations within a 30 m×30 m square and mixed the five samples thoroughly in the laboratory to represent the soil of that area. To determine the coordinates of the samples we used a handheld GPS receiver (MAP64SJZ, Garmin Ltd., Longmont, CO, USA).

The samples were taken to the Key Laboratory of Desert and Desertification at the Northwest Institute of Eco-Environment and Resources, Chinese Academy of Sciences, for chemical analysis and spectral reflectance measurement. Samples were air-dried, ground and sieved (1-mm mesh) to remove large particles and plant residues. They were then analysed for electrical conductivity, pH, organic matter content (OMC), and soluble salt content (Na^+ , K^+ , Ca^{2+} , Mg^{2+} , Cl^- , SO_4^{2-} , CO_3^{2-} and HCO_3^-). The electrical conductivity was measured using soil over water mass ratio of 1:5. The pH was measured using soil over water mass ratio of 1:1 (Thomas et al., 1996). The amounts of Na^+ , K^+ , Ca^{2+} , Mg^{2+} , Cl^- and SO_4^{2-} in samples were measured using an ion chromatograph (Dionex ICS-900, Thermo Fisher Scientific Inc., Waltham, USA). Amounts of CO_3^{2-} and HCO_3^- were measured using the double indicator titration method. The total soluble salt content (SSC) of each sample was determined on the basis of the total mass of the eight ionic concentrations (Bao, 2000). The soil samples were further sieved to isolate the <0.1-mm size fraction to measure organic carbon content (OCC).

To determine the spectral characteristics of different levels of soil salinity, we divided the spectra of the 64 soil samples into five salinity ranges as follows: 8 samples, 4–10 g/kg; 14 samples, 10–21 g/kg; 9 samples, 21–30 g/kg; 19 samples, 30–40 g/kg; and 14 samples, 40–52 g/kg (Wang, 1993).

2.3 Spectral data measurements

Spectral measurements were conducted in a dark room with one halogen lamp (Lowe Light Pro, JCV 14.5V-70WC) illuminating the sample from a nadir position 20 cm to ensure stable atmospheric and uniform illumination conditions (Zhang et al., 2013). We used a spectroradiometer (FieldSpec 4, Analytical Spectral Devices Inc., Longmont, USA) to acquire reflectance spectra of the soil samples at wavelengths between 350 and 2500 nm. The spectroradiometer uses individual detector arrays to record spectra at VNIR (350–1050 nm), SWIR1 (1000–1800 nm) and SWIR2 (1800–2500 nm) wavelengths. Sampling intervals were 1.4 nm for wavelengths 350–1000 nm (spectral resolution 3.0 nm) and 2.0 nm for wavelengths 1000–2500 nm (spectral resolution 10.0 nm); thus, spectral resolution varied from 3.0 nm for the shortest wavelengths to 10.0 nm for the longest wavelengths (Danner et al., 2015).

Reflectance data were collected using a fibre optic probe with a 25° field of view that was installed on a tripod about 30 cm above the target and at about 15° off nadir, which provided an observed surface area of 177 cm². Each soil sample was filled to overflowing in a Petri dish (10 cm diameter, 1 cm thick) and the upper surface was scraped off to provide a flat surface (Zhang, 2014). To minimize instrument noise, the reflectance were measured for 20 times and averaged to obtain the mean spectra for each soil sample. Before each measurement, reflectance was calibrated against a white reference panel of known reflectance (LapSphere Spectralon Diffuse Reflectance Panel) (Farifteh et al., 2008).

2.4 Spectrum data processing

Sensory errors inherent in the analytical spectral devices (ASD) spectroradiometer caused splices at around 1000 and 1800 nm. These errors were corrected by applying the ASD ViewSpecPro program to smooth the "splices" between detector array domains (Danner et al., 2015).

A continuum-removal (CR) algorithm (ENVI image processing package, Research Systems Inc., Boulder, USA) was applied to all of the saline soil spectra that we measured to enhance small absorption features and better discriminate subtle differences in spectral features among samples (Clark and Roush, 1984; Huang et al., 2004). The continuum is a convex "hull" of line segments

fitted along the top of a spectrum curve to connect local spectral maximums and represents the baseline. Against the baseline, more subtle absorption features are evident (Clark and Roush, 1984; Huang et al., 2004; Farifteh et al., 2008). The reflectance value at each point in an absorption feature was divided by the reflectance level of the corresponding convex hull to remove continuums for each waveband; the resulting ratio is known as CR-reflectance (Huang et al., 2004). We also determined a mean spectrum of CR-reflectance to represent the basic spectral characteristics of the five ranges of soil salinity defined in Section 2.2.

2.5 Selection of sensitive bands

We developed a normalized difference salinity index (NDSI; Eq. 1) to predict soil salinity from CR-reflectance data.

$$\text{NDSI}_{i,j,n} = (\text{CRR}_{i,n} - \text{CRR}_{j,n}) / (\text{CRR}_{i,n} + \text{CRR}_{j,n}), \quad (1)$$

where n is the number of soil samples and CRR is the CR-reflectance of sample n for arbitrary wavebands i and j .

The NDSI, composed of two arbitrary waveband components in the 350–2500 nm (2151 wavebands in total) wavelength range, provided 2,312,325 candidate pairs for the 64 samples. Using one pair of waveband, the 64 samples obtained 64 NDSI values. For the 64 samples, the correlation analysis (Eq. 2) was then applied to the NDSI and SSC; we likewise used correlation analysis to evaluate the relationships between the candidate NDSI waveband pairs and the known SSC.

$$r = \frac{\sum_{i=1}^n (\text{NDSI}_{i,j} - \overline{\text{NDSI}_{i,j}}) (\text{SSC}_i - \overline{\text{SSC}})}{\sqrt{\sum_{i=1}^n (\text{NDSI}_{i,j} - \overline{\text{NDSI}_{i,j}})^2 \sum_{i=1}^n (\text{SSC}_i - \overline{\text{SSC}})^2}}, \quad (2)$$

where r is the correlation coefficient between NDSI and SSC, n is the number of soil samples, $\text{NDSI}_{i,j}$ is the CR-reflectance of the spectrum for the j^{th} band of the i^{th} sample, SSC_i is the soluble salt content of the i^{th} sample, and $\overline{\text{NDSI}_{i,j}}$ and $\overline{\text{SSC}}$ are the means of NDSI and soluble salt content, respectively.

The correlation coefficients between SSC values and all possible candidate NDSI were used to evaluate the contribution of NDSI to the estimation of soil salinity. The pair of bands with the highest correlation coefficient were taken to be the pair with the greatest sensitivity to soil salinity.

2.6 Modelling the relationship between NDSI and SSC

Among the 64 soil samples, we used 33 samples to establish a linear model of the relationship between NDSI and SSC by univariate regression with measured SSC as the dependent variable and NDSI as the independent variable. The measured SSC of the remaining 31 samples were used to validate the model.

3 Results and discussion

3.1 Descriptive statistics of soil chemical properties

Descriptive statistics on the chemical properties of the 64 soil samples are presented in Table 1. The soil samples showed a broad range of salinity from 4.07 to 51.26 g/kg (median, 31.54 g/kg). The predominant anions in the samples were SO_4^{2-} and Cl^- and the predominant cations were Na^+ and Ca^{2+} .

The correlation coefficients were 0.295 between SO_4^{2-} and Na^+ , 0.800 between Cl^- and Na^+ , and 0.789 between Cl^- and Ca^{2+} (Table 2). There were also strong correlations of SSC with Ca^{2+} ($r=0.854$), Cl^- ($r=0.695$) and SO_4^{2-} ($r=0.587$). Thus, it is likely that most of the chemical compounds in the soil samples are chlorine and sulphate compounds.

Although both K^+ and Mg^{2+} showed strong positive relationships with Cl^- and SSC, which might indicate the presence of KCl or MgCl_2 , their very low mean concentrations (0.15 and 0.29 g/kg for

K^+ and Mg^{2+} , respectively) indicate that KCl and $MgCl_2$ were not dominant salts in the soil samples.

There were very low contents of HCO_3^- in the soil samples and no CO_3^{2-} was identified, which together indicate that there was little in the way of bicarbonate compounds and no discernible carbonate compounds in the soils.

The dominant anions in each of the five salinity ranges were SO_4^{2-} and Cl^- (Fig. 2). The concentration of bicarbonate decreased with increasing soil salinity. As soil salinity increased, Na^+ became the dominant cation for the SSC ranges of 21–30, 30–40 and 40–52 g/kg. The concentrations of Ca^{2+} were relatively high for all salinity ranges, which indicates that the dominant salts were probably $CaSO_4$ and $CaCl_2$ for the lower salinity samples (SSC of 4–10 and 10–21 g/kg).

Table 1 Descriptive statistics of chemical properties of the 64 soil samples

Statistic	Na^+	K^+	Mg^{2+}	Ca^{2+}	Cl^-	SO_4^{2-}	HCO_3^-	CO_3^{2-}	$EC_{1:5}$	SSC	OCC
	(g/kg)								(mS/cm)	(g/kg)	
Max	20.84	0.51	2.07	4.76	17.80	40.56	0.34	0.00	22.36	51.26	7.36
Min	0.00	0.03	0.01	0.05	0.68	2.37	0.01	0.00	0.14	4.07	2.22
Mean	4.13	0.15	0.29	2.11	5.70	15.50	0.14	0.00	5.59	28.01	4.83
SD	5.50	0.12	0.37	1.56	4.28	9.60	0.05	0.00	5.61	13.34	1.16
CV	1.33	0.77	1.30	0.74	0.75	0.62	0.39	0.00	1.00	0.48	0.24

Note: SD, standard derivation; CV, coefficient of variance (ratio of standard derivation to the mean); $EC_{1:5}$, electrical conductivity at a soil water ratio of 1:5; SSC, soluble salt content; OCC, organic carbon content.

Table 2 Correlation matrix of relationships between variables

	Na^+	K^+	Mg^{2+}	Ca^{2+}	Cl^-	SO_4^{2-}	HCO_3^-	$EC_{1:5}$	SSC
Na^+	1.000								
K^+	0.815**	1.000							
Mg^{2+}	0.668**	0.550**	1.000						
Ca^{2+}	0.782**	0.759**	0.661**	1.000					
Cl^-	0.800**	0.724**	0.718**	0.789**	1.000				
SO_4^{2-}	-0.285*	-0.108	-0.128	0.195	-0.100	1.000			
HCO_3^-	-0.049	0.140	0.004	-0.006	0.110	-0.125	1.000		
$EC_{1:5}$	0.961**	0.795**	0.717**	0.806**	0.817**	-0.230	-0.062	1.000	
SSC	0.579**	0.601**	0.522**	0.854**	0.695**	0.587**	-0.074	0.611**	1.000

Note: **, significant at the 0.01 probability level (2-tailed); *, significant at the 0.05 probability level (2-tailed).

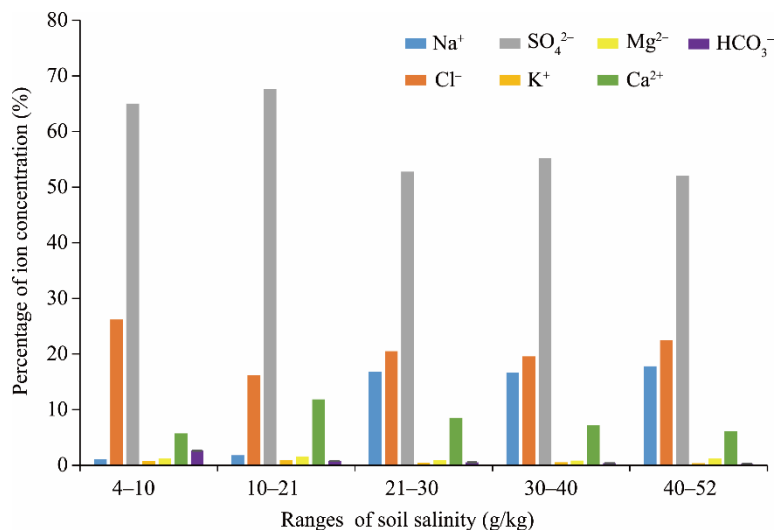


Fig. 2 Concentrations of Na^+ , K^+ , Ca^{2+} , Mg^{2+} , Cl^- , SO_4^{2-} and HCO_3^- ions for different ranges of soil salinity. The percentage of ion concentration was calculated by dividing the concentration of certain ion by the total cation and anion concentration of the corresponding soil salinity range.

For the higher salinity ranges (SSC of 21–30, 30–40, 40–52 g/kg), the dominant salts were probably NaCl, CaSO₄, CaCl₂ and NaSO₄. Concentrations of Ca²⁺ initially increased with increasing soil salinity up to 20 g/kg, but then decreased with further increases of salinity. The concentration of HCO₃⁻ decreased as soil salinity increased across the entire salinity range (Fig. 2).

3.2 Spectral features of soil samples

The spectra of all 64 samples were of similar shapes with considerable overlap (Fig. 3a). The representative spectra for the five ranges of salinity (Fig. 3b) exhibited several differences in the width of reflectance peaks and depth of absorption troughs. CR-processing of the spectra strengthened the peaks and troughs of these spectra (Figs. 3c and d). The spectra for samples in each of the five salinity ranges showed similar absorption features at wavelengths of about 1400, 1900 and 2200 nm. These features are associated with the particular salts in the soils and are related to the internal vibrational processes of anions (e.g., OH⁻, SO₄²⁻ and the Al-OH group) or to water

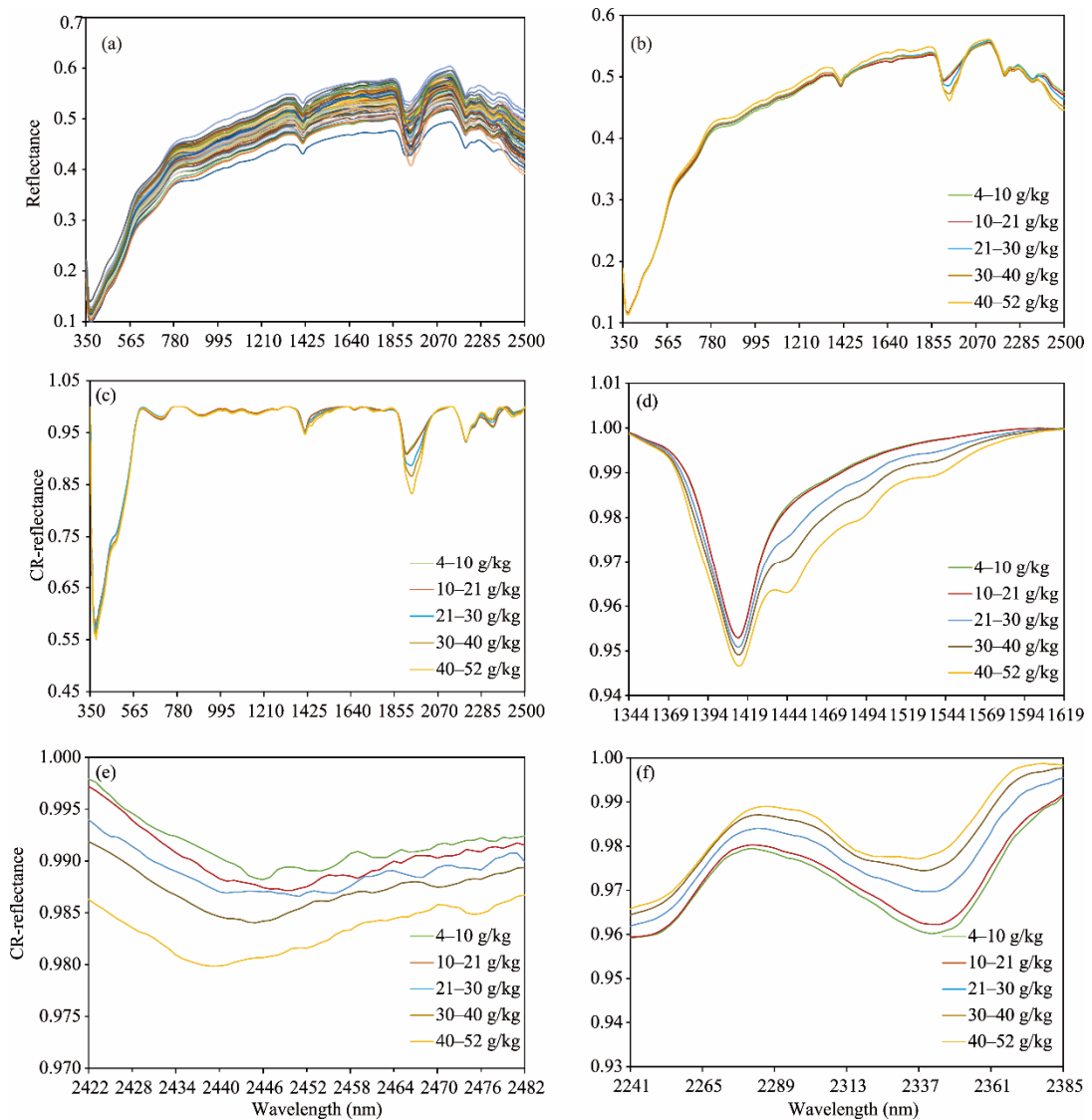


Fig. 3 Reflectance spectra: (a) original measured spectra of all 64 soil samples, (b) averaged spectra of samples in five salinity ranges, (c) CR-reflectance spectra of samples in five salinity ranges, (d) enlargement of panel for range of 1344–1619 nm, (e) enlargement of panel for range of 2422–2482 nm, and (f) enlargement of panel for range of 2241–2385 nm.

molecules that are trapped in or adsorbed on the crystal structure (Hunt, 1977; Crowley, 1991). The internal vibrational processes of the anion groups were the result of overtones or combinations (stretching and bending modes) of fundamental vibrations and of vibrations of the entire lattice (Hunt, 1977; Mougenot et al., 2009). The broad absorption features near 1400, 1940 and 2250 nm are probably related to fluid inclusions in halite (NaCl) after drying (Clark and Roush, 1984; Crowley, 1991; Danner et al., 2015). The features near 2200, 2300 and 2400 nm probably represent O-H stretch, AlOH/MgOH bending mode, or the combined effect of both. Previous research has shown that these salt minerals (e.g., chlorine compounds) are the dominant evaporites that form crystals or efflorescence in salinized crusts and scalds in arid regions (Farifteh et al., 2008). Moreover, previous researchers suggested that absorption features at around 1000, 1200, 1400, 1600, 1740, 1900, 2200 and 2330 nm might also be affected by combination overtones of O-H stretching, H-O-H bending fundamentals, and various overtones in gypsum ($\text{CaSO}_4 \cdot 2\text{H}_2\text{O}$) (Howari et al., 2002).

In the range from 350 to 1000 nm, no marked difference was distinguishable among the spectra for the five salinity ranges (Fig. 3c). At wavelengths higher than 1300 nm, salinity-induced changes in soil reflectance were evident, particularly in the water absorption bands at around 1400 and 1900 nm (Fig. 3c). Reflectances of the lower salinity ranges were higher than those of the higher salinity ranges at about 1344–1619 nm (Fig. 3d) and 2422–2482 nm (Fig. 3e). In contrast, reflectances of the higher salinity ranges were higher than those of the lower salinity ranges near a small peak at 2241–2385 nm (Fig. 3f). The depths of the absorption troughs centred at about 1410 and 1940 nm, increased with increasing salinity.

3.3 Modeling of SSC and model validation

Correlation of the wavebands of measured salinities of 64 samples with all of the waveband pairs used in the NDSI (Fig. 4) produced strong correlations (absolute value of $r > 0.84$) for the following pairs: 750–920 and 2351–2487, 1199–1379 and 2351–2487, 1553–1765 and 2351–2487, and 2118–2261 and 2351–2487 nm (Fig. 4). Among these waveband pairs, the most promising sensitive waveband pairs were 1199–1379 and 2351–2487 nm. The bands including wavelengths 1358 and 2382 nm ($r = -0.87$) were identified as the most promising bands that can be used to develop a quantitative model for estimation of salt concentration from hyperspectral data.

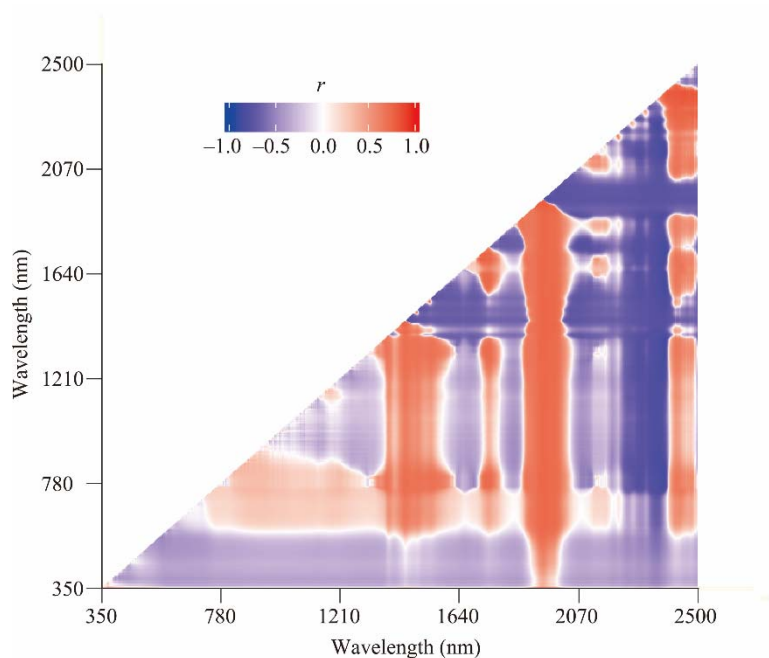


Fig. 4 Heatmap of correlation coefficients (r) for measured salinity with all candidate NDSI waveband pairs

We therefore defined the following salinity spectral index (SSI):

$$\text{SSI} = (\text{B2382} - \text{B1358}) / (\text{B2382} + \text{B1358}), \quad (3)$$

where B1358 and B2382 are CR-reflectances of spectral bands at 1358 and 2382 nm, respectively.

The model established by univariate linear regression to estimate SSC from hyperspectral data (Fig. 5a) was expressed as,

$$\text{SSC} = 5312.3 \times \text{SSI} + 34.187 \quad (r = 0.8272). \quad (4)$$

Validation of the predicted values of SSC against measured values (Fig. 5b) showed that Equation 5 over-estimated SSC, which we attributed to the presence in our samples of some salt ions (e.g., Fe and Al) that were not measured during laboratory analysis.

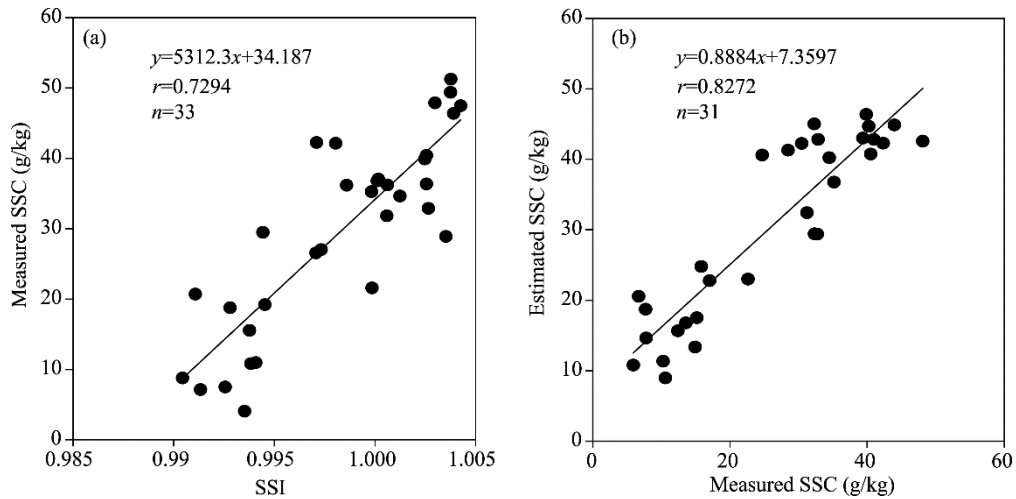


Fig. 5 (a) Measured soluble salt content (SSC) versus salinity spectral index (SSI) and (b) scatter plots of measured SSC versus SSC estimated from Equation 5

To ascertain which soluble salts the CR-reflectance wavelengths were responsive to, we examined the relationships of ionic concentrations (Na^+ , K^+ , Ca^{2+} , Mg^{2+} , Cl^- , SO_4^{2-} , CO_3^{2-} and HCO_3^-) in the 64 samples with the CR-reflectances at 2382 and 1358 nm, and with the SSI (Fig. 6). We found significant correlations between Na^+ and the CR-reflectances at 2382 ($r=0.622$) and 1358 nm ($r=-0.603$), between Na^+ and SSI ($r=0.661$), between Cl^- and the CR-reflectances at 2382 ($r=0.683$) and 1358 nm ($r=-0.561$), and between Na^+ and SSI ($r=0.711$). Howari et al. (2002) reported that distinct absorption features for $\text{CaSO}_4 \cdot 2\text{H}_2\text{O}$, mixture of $\text{CaSO}_4 \cdot 2\text{H}_2\text{O}$ and NaCl , and NaHCO_3 were occurred at wavelenghtes of 1199–1379 nm. For the wavelenghtes of 2351–2487 nm, absorption band position reported by Crowley (1991) and Howari et al. (2002) were related with NaHCO_3 and $\text{CaSO}_4 \cdot 2\text{H}_2\text{O}$. These results indicate that the two bands used in this study to construct the SSI were best suited for soils where the predominant soluble salts contain chlorine, sulphate and carbonate compounds. In contrast, in the Yellow River delta region of China where the dominant soluble salts are NaCl and MgCl_2 , CR-reflectances at 2052 and 2203 nm were used to construct a spectral soil salinity index (Weng et al., 2010). In South Africa, where most of the salts in soils are of marine origin, reflectances at 2040 and 1410 nm were identified as the most promising for use in a spectral soil salinity index (Mashimbye, 2013). Considering our results and those from other regions, it is evident that particular salts influence spectral reflectance differently, so the wavelengths employed in developing SSI should be selected on a case by case basis, although a particular SSI may be applicable in areas with the same salt types as the area in which the SSI was developed. In addition, the lab measured spectral reflectance of air-dried soil samples avoid the interference of moisture content, surface roughness and vegetation, etc. Thus, the accuracy of soil salinity estimation has been improved. However, for remote sensing data based large-scale salinity monitoring, the spectra of saline soils vary largely with moisture content, roughness and other soil surface features, which may cause significant errors during soil salt content estimation.

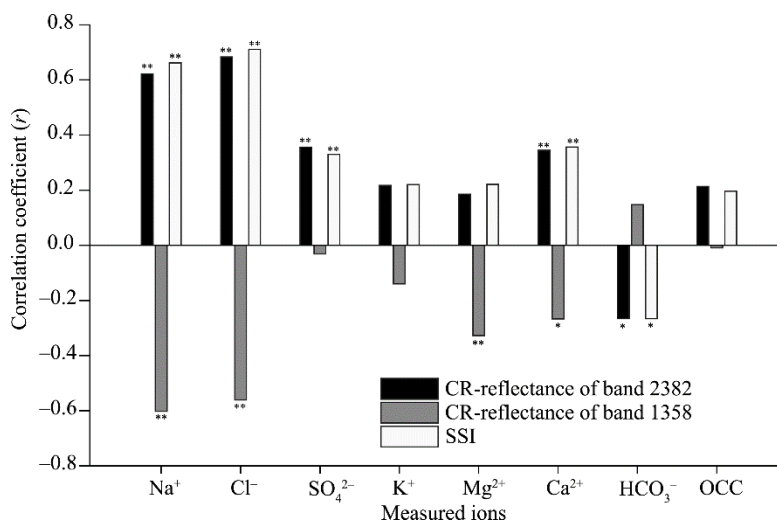


Fig. 6 Correlation coefficients (r) obtained for measured concentrations of seven ions and organic carbon content (OCC) with the CR-reflectances at 2382 and 1358 nm, and with the salinity spectral index (SSI). **, correlation significant at the 0.01 probability level (2-tailed). *, correlation significant at the 0.05 probability level (2-tailed).

4 Conclusions

Statistical analysis of the measured soluble salt contents and the lab measured hyperspectral reflectance for all of the 64 soil samples showed that two wavebands centred at 2382 and 1358 nm were closely associated with sodium and chloride concentrations and thus were selected as optimal wavebands. NDSI was developed and used as the independent variable in the modelling process based on the optimal wavebands. The validation of the model showed a strong correlation ($r=0.8272$). Thus, the model we derived successfully estimated the soluble salt content of surface soils in the study area in which the dominant salt types are chlorine and sulphate compounds. Further research is needed on the application of this method to remotely sensed (aircraft or satellite) digital hyperspectral data so that its potential use for large-scale predictive mapping of the extent and severity of soil salinity can be investigated.

Acknowledgements

This research was supported by the International Platform for Dryland Research and Education, Tottori University and the National Key R&D Program of China (2016YFC0500909). The authors would like to thank Professor WEI Huaidong, Professor DING Feng and Professor ZHOU Liping from Gansu Desertification and Aeolian Sand Disaster Combating Institute for providing the equipment and assistance in the measurement; Professor XUE Xian, Professor WANG Ninglian, Dr. HUANG Cuihua, Dr. LIAO Jie, Dr. LUO Jun and Dr. DONG Siyang from Northwest Institute of Eco-Environment and Resources, Chinese Academy of Sciences, for providing the equipment and the assistance in the field work; and Professor Kitamura YOSHINOBU and Fujimaki HARUYUKI from Tottori University for their helpful advices and providing the equipment for experiments.

References

- Bao S D. 2000. Soil Agricultural Chemistry Analysis. Beijing: China Agriculture Press, 178–198. (in Chinese)
- Barrett-Lennard E G. 2003. The interaction between waterlogging and salinity in higher plants: causes, consequences and implications. *Plant and Soil*, 253(1): 35–54.
- Ben-Dor E, Banin A. 1995. Near-infrared analysis as a rapid method to simultaneously evaluate several soil properties. *Soil Science Society of America Journal*, 59(2): 364–372.
- Ben-Dor E, Chabrilat S, Demattê J A M, et al. 2009. Using imaging spectroscopy to study soil properties. *Remote Sensing of Environment*, 113(Suppl. 1): S38–S55.
- Bondes M, Li D. 2013. Climate Change and Sustainable Development in Western China's Minqin Oasis: Joining Forces with

- Society. In: Vajpeyi D. Climate Change, Sustainable Development and Human Security. New York: Lexington, 139–168.
- Chen L, Feng Q, Li C, et al. 2016. Spatial variations of soil microbial activities in saline groundwater-irrigated soil ecosystem. *Environmental Management*, 57(5): 1054–1061.
- Clark R N, Roush T L. 1984. Reflectance spectroscopy: Quantitative analysis techniques for remote sensing applications. *Journal of Geophysical Research: Solid Earth*, 89(B7): 6329–6340.
- Crowley J K. 1991. Visible and near-infrared (0.4–2.5 μm) reflectance spectra of Playa evaporate minerals. *Journal of Geophysical Research: Solid Earth*, 96(B10): 16231–16240.
- Danner M, Locherer M, Hank T, et al. 2015. Spectral Sampling with the ASD FieldSpec 4-Theory, Measurement, Problems, Interpretation. In: EnMAP Field Guides Technical Report. GFZ Data Services. Brandenburg, Germany.
- Dehaan R, Taylor G R. 2003. Image-derived spectral endmembers as indicators of salinisation. *International Journal of Remote Sensing*, 24(4): 775–794.
- Ding J L, Wu M C, Tiyyip T. 2011. Study on soil salinization information in arid region using remote sensing technique. *Agricultural Sciences in China*, 10(3): 404–411.
- Douaoui A E K, Nicolas H, Walter C. 2006. Detecting salinity hazards within a semiarid context by means of combining soil and remote-sensing data. *Geoderma*, 134(1–2): 217–230.
- Dwivedi R S. 2001. Soil resources mapping: A remote sensing perspective. *Remote Sensing Reviews*, 20(2): 89–122.
- Fan X, Liu Y, Tao J, et al. 2015. Soil salinity retrieval from advanced multi-spectral sensor with partial least square regression. *Remote Sensing*, 7(1): 488–511.
- Farifteh J, Farshad A, George R J. 2006. Assessing salt-affected soils using remote sensing, solute modelling, and geophysics. *Geoderma*, 130(3–4): 191–206.
- Farifteh J, Van der Meer F, Atzberger C, et al. 2007. Quantitative analysis of salt-affected soil reflectance spectra: A comparison of two adaptive methods (PLSR and ANN). *Remote Sensing of Environment*, 110(1): 59–78.
- Farifteh J, Van der Meer F, Van der Meijde M, et al. 2008. Spectral characteristics of salt-affected soils: A laboratory experiment. *Geoderma*, 145(3–4): 196–206.
- Fernández-Bucs N, Siebe C, Cram S, et al. 2006. Mapping soil salinity using a combined spectral response index for bare soil and vegetation: A case study in the former lake Texcoco, Mexico. *Journal of Arid Environments*, 65(4): 644–667.
- Goetz A F H. 2009. Three decades of hyperspectral remote sensing of the Earth: A personal view. *Remote Sensing of Environment*, 113(Suppl. 1): S5–S16.
- Gomez C, Viscarra Rossel R A, McBratney A B. 2008. Soil organic carbon prediction by hyperspectral remote sensing and field vis-NIR spectroscopy: An Australian case study. *Geoderma*, 146(3–4): 403–411.
- Haubrock S N, Chabrillat S, Kuhnert M, et al. 2008a. Surface soil moisture quantification and validation based on hyperspectral data and field measurements. *Journal of applied remote sensing*, 2(1): 1–26.
- Haubrock S N, Chabrillat S, Lemmertz C, et al. 2008b. Surface soil moisture quantification models from reflectance data under field conditions. *International Journal of Remote Sensing*, 29(1): 3–29.
- Howari F M, Goodell P C, Miyamoto S. 2002. Spectral properties of salt crusts formed on saline soils. *Journal of Environmental Quality*, 31(5): 1453–1461.
- Huang Z, Turner B J, Dury S J, et al. 2004. Estimating foliage nitrogen concentration from HYMAP data using continuum removal analysis. *Remote Sensing of Environment*, 93(1–2): 18–29.
- Hunt G R. 1977. Spectral signatures of particulate minerals in the visible and near infrared. *Geophysics*, 42(3): 501–513.
- Li J, Pu L, Han M, et al. 2014. Soil salinization research in China: Advances and prospects. *Journal of Geographical Sciences*, 24(5): 943–960.
- Lu P, Wang L, Niu Z, et al. 2013. Prediction of soil properties using laboratory VIS-NIR spectroscopy and Hyperion imagery. *Journal of Geochemical Exploration*, 132(Suppl. C): 26–33.
- Ma J Z, Wang X S, Edmunds W M. 2005. The characteristics of ground-water resources and their changes under the impacts of human activity in the arid Northwest China—a case study of the Shiyang River Basin. *Journal of Arid Environments*, 61(2): 277–295.
- Ma Y, Fan S, Zhou L, et al. 2007. The temporal change of driving factors during the course of land desertification in arid region of North China: the case of Minqin County. *Environmental Geology*, 51(6): 999–1008.
- Mashimbye Z E. 2013. Remote sensing of salt-affected soils. PhD Dissertation. Western Cape: Stellenbosch University, 98.
- Metternicht G I, Zinck J A. 2003. Remote sensing of soil salinity: potentials and constraints. *Remote Sensing of Environment*, 85(1): 1–20.
- Mougenot B, Pouget M, Epema G F. 1993. Remote sensing of salt affected soils. *Remote Sensing Reviews*, 7(3–4): 241–259.
- Munns R. 2002. Comparative physiology of salt and water stress. *Plant, Cell & Environment*, 25(2): 239–250.

- Qian T N, Tsunekawa A, Masunaga T, et al. 2017. Analysis of the Spatial Variation of Soil Salinity and Its Causal Factors in China's Minqin Oasis. *Mathematical Problems in Engineering*, Vol. 2017. <https://doi.org/10.1155/2017/9745264>.
- Rengasamy P. 2006. World salinization with emphasis on Australia. *Journal of Experimental Botany*, 57(5): 1017–1023.
- Sheng J, Ma L, Jiang P, et al. 2010. Digital soil mapping to enable classification of the salt-affected soils in desert agro-ecological zones. *Agricultural Water Management*, 97(12): 1944–1951.
- Shi X Z, Yu D S, Yang G X, et al. 2006. Cross-reference benchmarks for translating the Genetic Soil Classification of China into the Chinese Soil Taxonomy. *Pedosphere*, 16(2): 147–153.
- Thomas G W. 1996. Soil pH and soil acidity. In: Sparks R S L, Swift D. L. *Methods of Soil Analysis. Part 3-Chemical Methods*. Madison: Soil Science Society of America, 475–490.
- Wang Q, Li P, Chen X. 2012. Modeling salinity effects on soil reflectance under various moisture conditions and its inverse application: A laboratory experiment. *Geoderma*, 170: 103–111.
- Wang Y, Li Y, Xiao D. 2008. Catchment scale spatial variability of soil salt content in agricultural oasis, Northwest China. *Environmental Geology*, 56(2): 439–446.
- Wang Y, Deng C, Liu Y, et al. 2018. Identifying change in spatial accumulation of soil salinity in an inland river watershed, China. *Science of the Total Environment*, 621: 177–185.
- Wang Z. 1993. *Chinese Saline-Alkaline Soil*. Beijing: Science Press, 335. (in Chinese)
- Wei H, Li Y, Xu C D, et al. 2016. The process of cultivated land and water resource distribution changing in recent decades in upstream and downstream in Shiyang Inland River Basin in arid area of Northwest China. *Journal of Geoscience and Environment Protection*, 4(7): 166–171.
- Weng Y, Gong P, Zhu Z. 2010. A spectral index for estimating soil salinity in the Yellow River Delta Region of China using EO-1 Hyperion data. *Pedosphere*, 20(3): 378–388.
- Wild A. 2003. *Soils, Land and Food: Managing the Land during the Twenty-First Century*. Cambridge: Cambridge University Press, 84–85.
- Xiao D, Li X, Song D, et al. 2007. Temporal and spatial dynamical simulation of groundwater characteristics in Minqin Oasis. *Science in China Series D: Earth Sciences*, 50(2): 261–273.
- Zhang F, Tiyyip T, Ding J, et al. 2003. Studies on the reflectance spectral features of saline soil along the middle reaches of Tarim River: a case study in Xinjiang Autonomous Region, China. *Environmental Earth Sciences*, 69(8): 2743–2761.
- Zhang J. 2014. Salt-affected soil resources in China. In: Zhang J F. *Coastal Saline Soil Rehabilitation and Utilization Based on Forestry Approaches in China*. Berlin: Springer Science & Business Media, 9–13.
- Zhang L F, Yang S W, Zhang M W. 2014. Study on land use change in arid and semiarid region based on GIS and RS. *Information Technology Journal*, 13(8): 1567–1571.
- Zornoza R, Guerrero C, Mataix-Solera J, et al. 2008. Near infrared spectroscopy for determination of various physical, chemical and biochemical properties in Mediterranean soils. *Soil Biology and Biochemistry*, 40(7): 1923–1930.